Supplemental Document

optica

Near-octave lithium niobate soliton microcomb: supplement

ZHENG GONG, XIANWEN LIU, YUNTAO XU, AND HONG X. TANG*

Department of Electrical Engineering, Yale University, New Haven, Connecticut 06511, USA
**Corresponding author: hong.tang@yale.edu*

This supplement published with The Optical Society on 28 September 2020 by The Authors under the terms of the Creative Commons Attribution 4.0 License in the format provided by the authors and unedited. Further distribution of this work must maintain attribution to the author(s) and the published article's title, journal citation, and DOI.

Supplement DOI: https://doi.org/10.6084/m9.figshare.12815891

Parent Article DOI: https://doi.org/10.1364/OPTICA.400994

Near-octave lithium niobate soliton microcomb: supplemental materials

Zheng Gong[1], **Xianwen Liu**[1], **Yuntao Xu**[1], **and Hong X. Tang**[1,*]

[1] *Department of Electrical Engineering, Yale University, New Haven, CT 06511, USA*
[*] *Corresponding author: hong.tang@yale.edu*

Compiled August 15, 2020

This document provides supplementary information for the main manuscript titled "Near-octave lithium niobate soliton microcomb", which includes our experiment setup, device characterization, the derivation of coupled mode equations with both Raman and Kerr effects, the derivation of the intracavity pump mode threshold energy for the 1st SRS, and a scheme for microcomb $2f-3f$ self-referencing on LN thin film platform as well as discussion on further broadening the soliton bandwidth.

http://dx.doi.org/10.1364/optica.XX.XXXXXX

1. EXPERIMENT SETUP AND DEVICE CHARACTERIZATION

The schematic of our experimental setup for accessing soliton microcombs is illustrated in Fig. S1. The pump light is sourced by an external cavity laser (ECL) whose output wavelength λ_c can be programmatically scanned across the microring resonances. An erbium-doped fiber amplifier (EDFA) is employed to amplify the ECL's output to pump the microring. Before the pump light is coupled onto the chip, its polarization state can be adjusted by a fiber polarization controller (FPC). Subsequently, the output of the chip is recorded and analyzed with direct photodetection (PD_1), an optical spectrum analyzer (OSA) and a photodetector (PD_2) followed by an electrical spectrum analyzer (ESA), respectively. To monitor comb power, a fiber Bragg grating (FBG) is used to suppress the pump component of the output before the photodetector PD_2.

The measured TE-transmission spectrum of our device (with $H = 0.56\,\mu$m, $W = 1.45\,\mu$m and $R = 60\,\mu$m) which produced the 4/5-octave spanning soliton microcombs (Fig. 2 in the main text) is partly presented in Fig. S1, where the TE00 resonances are indicated by the dips. The intrinsic decay rate and external coupling rate of the pump mode can be extracted by fitting the linewidth of the resonance (Fig. S1) and estimated to be $\kappa_i/(2\pi) = 190$ MHz and $\kappa_e/(2\pi) = 250$ MHz. The top width of the coupling waveguide is 0.8 μm and the coupling gap is 0.8 μm. To access the soliton state, we tuned the pump frequency into the resonance from its red-side until the soliton mode-locking was triggered under photorefractive effect [1, 2], signaled by the emergence of steady-steps in the comb power trace (Fig. S1(d)). When the pump was scanned out of the existence range of the soliton states [3], the cavity entered into chaotic comb states [1, 2], as manifested by the fluctuations in the comb power trace (Fig. S1(d)). The soliton comb exhibited low noise compared with the MI comb, as indicated by the measured relative intensity noise spectra (Fig. S1(e)).

2. DERIVATION OF COUPLED MODE EQUATIONS WITH RAMAN AND KERR EFFECTS IN A MICRORING

The intracavity Kerr four-wave mixing can be described by an interaction Hamiltonian as

$$\mathcal{H}_K = g_K \delta(i+j-k-l) \sum_{ijkl} a_i^\dagger a_j^\dagger a_k a_l, \tag{S1}$$

where a is the annihilation operator for the photon modes, with the subscripts j, k, l denoting the angular momentum of these operators. g_K represents the Kerr nonlinear coupling strength [3]. The phase-matching condition is reflected by the δ-function.

We treat the intracavity Raman scattering as a second-order nonlinear process between two photon modes and one Raman-active phonon mode, which can be represented by

$$H_R = \sum_{j,k,l} g_R^{ijk} \left(a_j^\dagger a_k R_l + a_j a_k^\dagger R_l^\dagger \right), \tag{S2}$$

where R is the annihilation operator for the phonon modes, and the Raman coupling strength is given by

$$g_R^{ijk} \propto \epsilon_0 \chi_R \int\int u_{x,j}(r,z)\, u_{x,k}(r,z)\, \boldsymbol{l_0} \delta(j-k-l). \tag{S3}$$

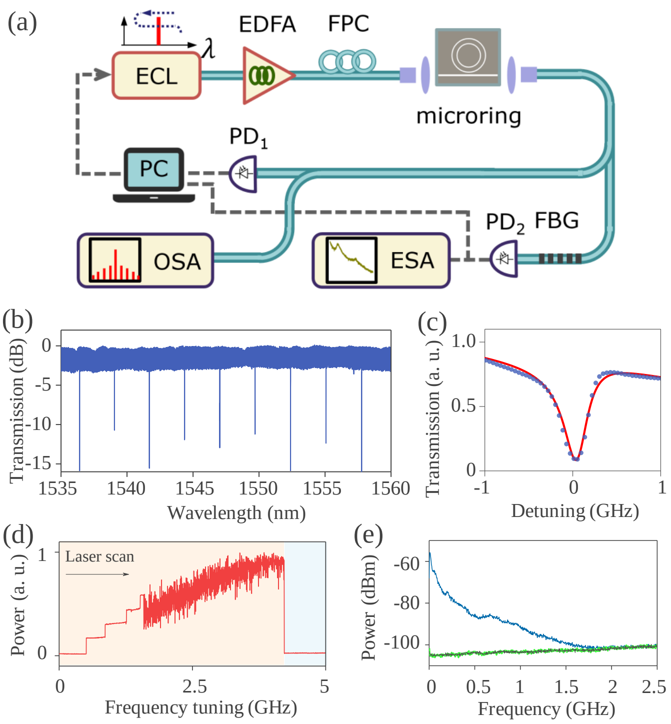

Fig. S1. (a) Schematic of the experiment setup. Cyan lines: optical fibers. Dashed gray lines: electrical cables. Component descriptions are in the text. (b) The measured TE-polarized transmission spectrum of the microring used for Fig. 2 in the main text. (c) Zoom-in view of a TE00 mode (blue dots) with a fitting curve (red). (d) Comb power trace under laser scan, which is the same as Fig. 2(c) in the main text and re-plotted here to facilitate illustrating (e). (e) Relative intensity noise spectra of a MI comb (blue), a soliton comb (green) and the detector background (black).

χ_R describes the Raman scattering tensor, and $u(r,z)$ is the photon mode distribution. We assume that $g_R^{ijk} = g_R$ is invariant over the frequencies of interest.

Considering both Kerr four-wave mixing and Raman scattering, the total Hamiltonian can be written as

$$\mathcal{H} = \mathcal{H}_{\text{sys}} + \mathcal{H}_{\text{K}} + \mathcal{H}_{\text{R}}, \tag{S4}$$

with

$$\mathcal{H}_{\text{sys}} = \sum_i \omega_{a,i} a_i^\dagger a_i + \sum_j \omega_{R,j} R_j^\dagger R_j, \tag{S5}$$

where ω_a and ω_R are the oscillating frequencies of the photon modes and the phonon modes respectively.

Based on Eq. (S4) and considering the system's intrinsic losses and external couplings, the dynamics of the mean fields of both the photon modes and phonon modes can be derived as follows

$$\frac{d}{dt}a_\mu = -(\kappa_\mu/2 + i\Delta_{a,\mu})a_\mu + ig_{\text{K}}\Big[\sum_{k,l,n} a_k^* a_l a_n \delta(l+n-k-\mu)\Big]$$
$$-ig_{\text{R}}\Big[\sum_{k,l} R_k a_l \delta(l+k-\mu)\Big] - ig_{\text{R}}\Big[\sum_{k,l} R_k^* a_l \delta(l-k-\mu)\Big] + \mathcal{E}_{\text{P}}, \tag{S6}$$

$$\frac{d}{dt}R_\mu = -(\gamma_{\text{R}}/2 + i\Delta_{R,\mu})R_\mu - ig_{\text{R}}\Big[\sum_{k,l} a_k^\dagger a_l \delta(l-k-\mu)\Big], \tag{S7}$$

where $\Delta_{a,\mu} = \text{D}_{\text{int},\mu} + \omega_0 - \omega_{\text{P}}$ (ω_0 is the cold cavity angular frequency of the pump mode), $\Delta_{R,\mu} = \omega_{\text{R}} - \mu D_1$ (D_1 represents the free spectral range). The total decay rate for the μ^{th} photon mode consists of the intrinsic decay rate and the coupling rate to the external waveguide, $\kappa_\mu = \kappa_{\text{i},\mu} + \kappa_{\text{e},\mu}$. The decay rate for the phonon mode is γ_{R}. The driving strength is denoted by $\mathcal{E}_{\text{P}} = \delta(\mu)\sqrt{\frac{\kappa_{\text{e},0}P_{\text{in}}}{\hbar\omega_{\text{P}}}}$ under an on-chip pump power of P_{in}. The computation time can be reduced by adopting the Fast Fourier Transform algorithm (FFT) [4] to calculate the summations. In the meantime, taking into account the fact that the phonon decay rate γ_{R} is much larger than the photon decay rate κ_μ, it is reasonable to adiabatically eliminate the phonon mode by setting the time derivative $\frac{d}{dt}\text{R}_\mu$ to zero to speed up the calculation. Note that Eqs. (S6, S7) only consider the dominant Raman mode which is centered at $\omega_{\text{R}}/(2\pi) \approx 18.75\,\text{THz}$ with an FWHM of $\gamma_{\text{R}}/(2\pi) \approx 558\,\text{GHz}$, as discussed in the following section. Couplings to multiple Raman modes can also be added similarly.

3. DERIVATION OF THE INTRACAVITY PUMP MODE THRESHOLD ENERGY FOR THE FIRST-ORDER SRS

We define the SRS threshold as the minimum intracavity pump mode energy $\varepsilon_{\text{R,th}}$ to initiate the first-order SRS, where the Stokes wave was observed to be $\sim 18.75\,\text{THz}$ away from the pump in the experiment. Neglecting Kerr four-wave mixing, the Hamiltonian for the first-order SRS from the pump mode follows

$$\mathcal{H} = \omega_a a^\dagger a + \omega_b b^\dagger b + \omega_{\text{R}} R^\dagger R + g_{\text{R}}\left(b^\dagger R^\dagger a + bRa^\dagger\right)$$
$$+ i\sqrt{\kappa_{\text{e},a}}\varepsilon_{\text{p}}\left(a^\dagger e^{-i\omega_{\text{p}}t} - ae^{i\omega_{\text{p}}t}\right), \tag{S8}$$

where a and b are the bosonic operators for the pump and Stokes modes, R represents the Raman-active phonon mode and the driving strength is $\varepsilon_{\text{p}} = \sqrt{P_{\text{in}}/\hbar\omega_{\text{p}}}$. In the rotating frame of $\omega_{\text{p}} a^\dagger a + \omega_b b^\dagger b + (\omega_{\text{p}} - \omega_b) R^\dagger R$, the cavity field in mode a can be written as the sum of the mean field α and the operator a, $a = \alpha + a$. By neglecting the fluctuation in mode a and considering the system's intrinsic losses and external couplings, we have

$$\frac{d}{dt}\alpha = (-i\delta_a - \kappa_a/2)\,\alpha - ig_{\text{R}}bR + \sqrt{\kappa_{\text{e},a}}\varepsilon_{\text{p}}, \tag{S9}$$

$$\frac{d}{dt}b = (-\kappa_b/2)b - ig_{\text{R}}\alpha R^\dagger + \sqrt{\kappa_b}b_{\text{in}}, \tag{S10}$$

$$\frac{d}{dt}R = (-i\delta_{\text{R}} - \gamma_{\text{R}}/2)\,R - ig_{\text{R}}\alpha b^\dagger + \sqrt{\gamma_{\text{R}}}R_{\text{in}}, \tag{S11}$$

where b_{in} is the input noise due to its coupling with the environment modes and the same for R_{in}. By using Fourier Transform

$$o(\omega) = \int dt o(t)\, e^{i\omega t}, \tag{S12}$$

$$o^\dagger(-\omega) = \int dt o^\dagger(t)\, e^{i\omega t}, \tag{S13}$$

we obtain

$$\alpha(\omega) = \frac{ig_{\text{R}}\int dt e^{i\omega t} b(t)\, R(t) - \sqrt{\kappa_{\text{e},a}}\varepsilon_{\text{p}}}{-i(\delta_a - \omega) - \kappa_a/2}\delta(\omega), \tag{S14}$$

$$b\left(\omega\right)=-\frac{\sqrt{\kappa_b}b_{\mathrm{in}}\left(\omega\right)+ig_{\mathrm{R}}\alpha\frac{\sqrt{\gamma_{\mathrm{R}}}R_{\mathrm{in}}^{\dagger}(-\omega)}{\alpha_{\mathrm{R}}^{-}}}{\alpha_b^{+}-\frac{g_{\mathrm{R}}^2|\alpha|^2}{\alpha_{\mathrm{R}}^{-}}}, \tag{S15}$$

$$R\left(\omega\right)=-\frac{\sqrt{\gamma_{\mathrm{R}}}R_{\mathrm{in}}\left(\omega\right)+ig_{\mathrm{R}}\alpha\frac{\sqrt{\kappa_b}b_{\mathrm{in},0}^{\dagger}(-\omega)}{\alpha_b^{-}}}{\alpha_{\mathrm{R}}^{+}-\frac{g_{\mathrm{R}}^2|\alpha|^2}{\alpha_b^{-}}}, \tag{S16}$$

where $\alpha_b^+ = i\omega - \kappa_b/2 = \alpha_b^-$, $\alpha_{\mathrm{R}}^+ = -i\left(\delta_{\mathrm{R}} - \omega\right) - \gamma_{\mathrm{R}}/2$, $\alpha_{\mathrm{R}}^- = i\left(\delta_{\mathrm{R}} + \omega\right) - \gamma_{\mathrm{R}}/2$. Then, the power spectrum of the intracavity field of mode b is derived as

$$S_b\left(\omega\right)=\left\langle b^{\dagger}\left(\omega\right)b\left(\omega\right)\right\rangle=\frac{1}{2\pi}\frac{\gamma_{\mathrm{R}}g_{\mathrm{R}}^2|\alpha|^2\left(n_{th}+1\right)}{|\alpha_b^{+}\alpha_{\mathrm{R}}^{-}-g_{\mathrm{R}}^2|\alpha|^2|^2}$$

where n_{th} is the mean phonon number in the thermal reservoir of the phonon mode. The Raman lasing starts at the frequency (ω) where $S_a\left(\omega\right)$ is maximized, i. e. $\alpha_b^+\alpha_{\mathrm{R}}^- - g_{\mathrm{R}}^2|\alpha|^2 \rightarrow 0$ which leads to

$$-\omega\left(\delta_{\mathrm{R}}+\omega\right)+\kappa_b\gamma_{\mathrm{R}}/4 \quad = \quad g_{\mathrm{R}}^2|\alpha|^2, \tag{S17}$$

$$\omega\gamma_{\mathrm{R}}+\left(\delta_{\mathrm{R}}+\omega\right)\kappa_b \quad = 0 \quad . \tag{S18}$$

Therefore, the detuning between the lasing frequency and the cold cavity resonant frequency of the photon mode b is

$$\omega_{\delta} \quad = \quad -\frac{\delta_{\mathrm{R}}\kappa_b}{\gamma_{\mathrm{R}}+\kappa_b},$$

and the lasing threshold is

$$|\alpha_{th}|^2 \quad = \quad \frac{\kappa_b\gamma_{\mathrm{R}}}{4g_{\mathrm{R}}^2}\left[1+\frac{\left(2\delta_{\mathrm{R}}\right)^2}{\left(\gamma_{\mathrm{R}}+\kappa_b\right)^2}\right]. \tag{S19}$$

For $\kappa_{\mathrm{R}} \gg \kappa_b$, the threshold reduces to

$$\varepsilon_{\mathrm{R,th}}=|\alpha_{th}|^2=\frac{\kappa_b\gamma_{\mathrm{R}}}{4g_{\mathrm{R}}^2}\left[1+\frac{\left(2\delta_{\mathrm{R}}\right)^2}{\gamma_{\mathrm{R}}^2}\right]. \tag{S20}$$

Note that the pump mode energy will be clamped at $\hbar\omega_{\mathrm{P}}\gamma_{\mathrm{R}}\kappa_b[1+(\frac{2\delta_{\mathrm{R}}}{\gamma_R})^2]/4g_{\mathrm{R}}^2$ once the first-order SRS is initiated.

The minimal intracavity pump mode energy required by a single soliton with an FWHM of γ_{S} can be approximated as

$$\varepsilon_{\mathrm{S,th}}\simeq\frac{\hbar\omega_{\mathrm{P}}D_2}{4g_{\mathrm{K}}}[1+2(\frac{\kappa D_1}{\gamma_{\mathrm{S}}D_2})^2], \tag{S21}$$

neglecting the Raman effect and ignoring the 3$^{\mathrm{rd}}$-order dispersion and above [3]. g_{K} denotes the Kerr nonlinear coupling rate [3]. D_1 and D_2 ($>$0) represent the free spectral range of the microresonator and the 2$^{\mathrm{nd}}$-order dispersion. All modes are assumed to have the same decay rates, $\kappa = \kappa_{\mathrm{e}} + \kappa_{\mathrm{i}}$. The first term in Eq. (S21) represents the energy of the frequency component at ω_{P} of the pulse, and the second term denotes the energy of the CW background. The microring of $H = 0.56\,\mu$m, $W =$ 1.45 μm and $R =$ 60 μm possesses a $g_{\mathrm{K}}/(2\pi)$ ≈ 1.1 Hz ($n_2 = 1.8\times10^{-19}$ m^2/W [1]).

In the experiment, the threshold of the dominant first-order SRS and corresponding g_{R} were assessed in a straight-waveguide coupled microring ($H = 0.56\,\mu$m, $W = 1.45\,\mu$m and $R = 60\,\mu$m). The first-order Stokes powers under gradually increased pump powers (pumping at 1544.36 nm) were recorded and plotted in Fig. S2. The threshold of the first-order SRS was found to be $\sim$4 mW for both directions. As an example, the SRS spectra for both directions are shown in Fig. S2 under

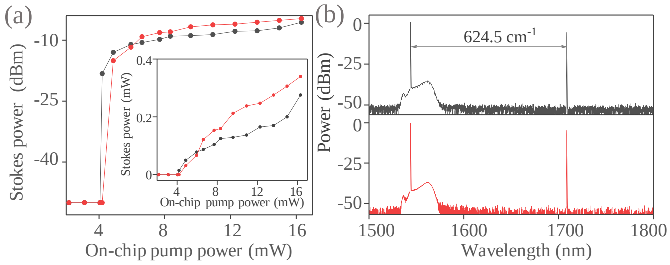

Fig. S2. (a) The measured off-chip Stokes powers in the forward (black) and backward (red) SRS versus on-chip pump powers. Inset: linear-scale plot. (b) The measured output spectra of the forward (black) and backward (red) SRS under an on-chip pump power of $\sim$16.3 mW.

a $\sim$16.3 mW on-chip pump power. The Stokes mode lasing at 1708.72 nm nearly overlapped with central Raman gain of E(LO$_8$) ($\delta_{\mathrm{R}} \approx 0$) [5]. The Raman gain has a frequency shift of 625 cm^{-1} ($\omega_{\mathrm{R}}/(2\pi) \approx 18.75$ THz) and an FWHM of 18.6 cm^{-1} ($\gamma_{\mathrm{R}}/(2\pi) \approx 558$ GHz) approximated by a Lorentz-profile [5]. By assuming that the Stokes mode exhibit the same κ_{e} and κ_{i} as the pump mode (Fig. S1) in this straight-waveguide coupled microring, g_{R} can be calculated from Eq. (S20) based on the measured threshold, which is 1.5 MHz. Additionally, the corresponding peak Raman gain coefficient is estimated to be 1.2 cm/GW based on [6].

To suppress Raman lasing in favor of soliton generation, it is essential to raise Raman lasing threshold $\varepsilon_{\mathrm{R,th}}$ above the soliton threshold $\varepsilon_{\mathrm{S,th}}$. Based on Eqs. (S20, S21), $\kappa_{\mathrm{e}} < 2.2\kappa_{\mathrm{i}}$ is required to promote the soliton generation in the microring studied in Fig. 2 of the main text. In the calculation, we assume that the modes exhibit uniform κ_{i} and κ_{e}, so that $\kappa_{\mathrm{b}} = \kappa = \kappa_{\mathrm{i}} + \kappa_{\mathrm{e}}$ in Eq. (S20). If the microring-waveguide coupling strength is not designed appropriately, SRS could dominate the cavity dynamics and prohibit the soliton generation. For example, Fig S3 shows a straight-wavegudie coupled microring of the same geometry and κ_{i} but with larger external coupling rate of $\kappa_{\mathrm{e}}/(2\pi) = 480$ MHz (coupling gap is 0.7 μm). The calculations based on Eqs. (S20, S21) suggest that the intracavity SRS threshold is lower than the threshold for generating a soliton with the same bandwidth obtained in Fig. 2(a), i. e. $\varepsilon_{\mathrm{R,th}}/\varepsilon_{\mathrm{S,th}} \approx 0.9$. For comparsion, Fig. 2(a) of the main text shows successful soliton generation with $\varepsilon_{\mathrm{R,th}}/\varepsilon_{\mathrm{S,th}} \approx 1.3$. As expected, no soliton steps showed up in the comb power trace (Fig. S3(b)), and no soliton combs other than the cascaded SRSs with local FWM were generated from this microring (Fig. S3(c)), when the pump was scanned across the resonance in the experiment.

4. SCHEME FOR SOLITON MICROCOMB SELF-REFERENCING ON LN THIN FILM PLATFORM

The spacing between the dual DWs of our soliton microcomb reaches 2/3 of an octave. Therefore, the soliton microcomb can in principle be self-referenced via the 2f-3f scheme [7]. Importantly, since LN is known to have strong $\chi^{(2)}$ nonlinearity, it is also possible to further integrate frequency doubling and tripling photonic elements on the same chip to realize on-chip microcomb self-referencing. One can conceive a single-chip implementation scheme for self-referenced microcomb generation shown in Fig. S4. A Mach-Zehnder interferometer (Elem. 1) is used to adjust $\mathrm{P_{in}}$ to tune the frequency offset of the soliton

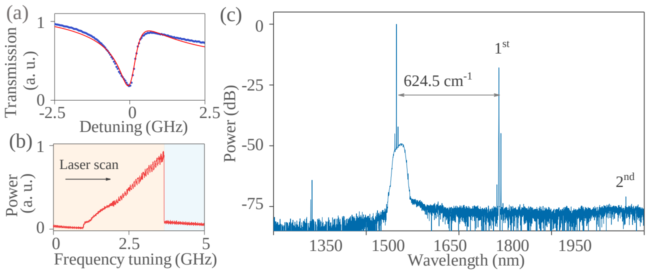

Fig. S3. (a) Zoom-in view of a TE00 pump resonance (blue dots) of the overly coupled microring with a fitting curve (red). (b) The measured comb power trace as the pump was scanned from the red-side (red shaded region) to the blue-side (blue shaded region) of the resonance at a speed of 62.5 GHz/s. An on-chip pump power of 280 mW was used, which is required to generate a soliton with an FWHM of 14 THz neglecting Raman effect [3]. (c) A normalized output spectrum from the overly coupled microring, obtained when the comb power reached near its maximum in (b).

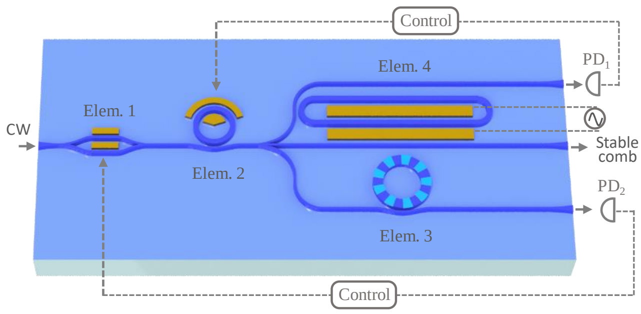

Fig. S4. (a) Schematic of the single-chip soliton microcomb self-referencing on the zcut LN thin film platform. The optical waveguides and electrodes are colored purple and yellow respectively. The descriptions of elements are in the text.

microcomb, known as f_{ceo} [8]. The microring (Elem. 2) for soliton microcomb generation is surrounded with electrodes which are employed to control the soliton microcomb FSR. A periodically poled microring (Elem. 3) for both efficient third and quasi-phase matched second harmonic generations creates RF beatings that contain f_{ceo} [7]. Additionally, a relatively long race-track microring (Elem. 4) together with electrodes form an electro-optic modulator serving the purpose of repetition rate division [9], which generates RF beatnotes within the photodetection bandwidth to monitor the soltion microcomb FSR. External tunable CW laser, photodetectors (PDs) and associated programs are used to facilitate the soliton excitation and feedback controls on stabilizing the f_{ceo} and FSR of the generated soliton microcomb.

In addition, we anticipate that further optimizing device fabrication to reduce the intrinsic decay rate κ_i [10] could facilitate generating broader soliton microcombs. For example, if $\kappa_i/(2\pi)$ drops by half, beyond octave-spanning (above OSA noise floor) soliton microcomb can be produced under the same on-chip pump power and dispersion profile D_{int} (Fig. S5). Note that the red-side DW becomes much stronger due to the reduced κ_i. As illustrated by the simulations in Fig.1 (c, e) of the main text, the D_{int} increases rapidly around the red-side DW in taller mi-

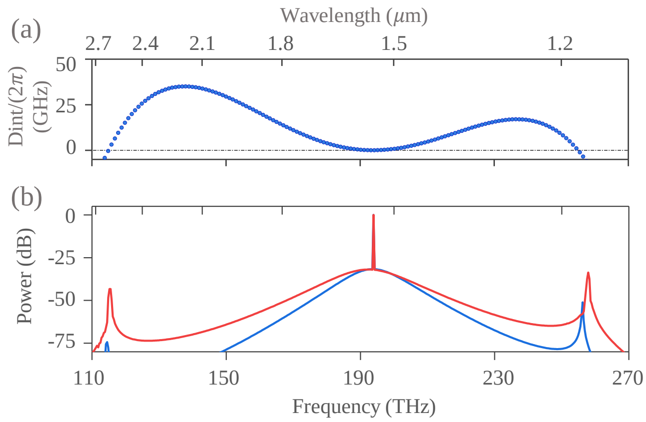

Fig. S5. (a) Simulated D_{int} for a microring with $H = 0.59\ \mu$m, $W = 1.45\ \mu$m and $R = 60\ \mu$m, which is the same as the curve in Fig. 1(c) of the main text. (b) Simulated soliton output spectra (normalized) for $\kappa_i = \kappa_e = 190$ MHz (blue) and $\kappa_i = \kappa_e = 95$ MHz (red). An on-chip pump power of 240 mW was used in both cases.

crorings, which renders the DW weak [11] and limits achievable microcomb bandwidth. Therefore, improving intrinsic Q_{in} is desired and would enable broader soliton microcomb generation.

REFERENCES

1. Y. He, Q.-F. Yang, J. Ling, R. Luo, H. Liang, M. Li, B. Shen, H. Wang, K. Vahala, and Q. Lin, "Self-starting bi-chromatic linbo3 soliton microcomb," Optica **6**, 1138–1144 (2019).
2. Z. Gong, X. Liu, Y. Xu, M. Xu, J. B. Surya, J. Lu, A. Bruch, C. Zou, and H. X. Tang, "Soliton microcomb generation at 2um in z-cut lithium niobate microring resonators," Opt. Lett. **44**, 3182–3185 (2019).
3. T. Herr, V. Brasch, J. D. Jost, C. Y. Wang, N. M. Kondratiev, M. L. Gorodetsky, and T. J. Kippenberg, "Temporal solitons in optical microresonators," Nat. Photonics **8**, 145–152 (2014).
4. T. Hansson, D. Modotto, and S. Wabnitz, "On the numerical simulation of kerr frequency combs using coupled mode equations," Opt. Commun. **312**, 134 – 136 (2014).
5. A. Ridah, P. Bourson, M. D. Fontana, and G. Malovichko, "The composition dependence of the raman spectrum and new assignment of the phonons in," J. Physics: Condens. Matter **9**, 9687–9693 (1997).
6. T. J. Kippenberg, S. M. Spillane, Bumki Min, and K. J. Vahala, "Theoretical and experimental study of stimulated and cascaded raman scattering in ultrahigh-q optical microcavities," IEEE J. Sel. Top. Quantum Electron. **10**, 1219–1228 (2004).
7. V. Brasch, E. Lucas, J. D. Jost, M. Geiselmann, and T. J. Kippenberg, "Self-referenced photonic chip soliton kerr frequency comb," Light. Sci. & Appl. **6**, e16202 (2017).
8. P. Del'Haye, A. Coillet, T. Fortier, K. Beha, D. C. Cole, K. Y. Yang, H. Lee, K. J. Vahala, S. B. Papp, and S. A. Diddams, "Phase-coherent microwave-to-optical link with a self-referenced microcomb," Na. Photonics **10**, 516 (2016).
9. S. B. Papp, K. Beha, P. Del'Haye, F. Quinlan, H. Lee, K. J. Vahala, and S. A. Diddams, "Microresonator frequency comb optical clock," Optica **1**, 10–14 (2014).
10. M. Zhang, C. Wang, R. Cheng, A. Shams-Ansari, and

M. Lončar, "Monolithic ultra-high-q lithium niobate microring resonator," Optica **4**, 1536–1537 (2017).

11. A. V. Cherenkov, V. E. Lobanov, and M. L. Gorodetsky, "Dissipative kerr solitons and cherenkov radiation in optical microresonators with third-order dispersion," Phys. Rev. A **95**, 033810 (2017).